Parameter Optimization of Nose Landing Gear Considering Both Take-off and Landing Performance of Catapult Take-off Carrier-Based Aircraft

Zhang Ming[1*], *Nie Hong*[1,2], *He Zhihang*[1]

1. Key Laboratory of Fundamental Science for National Defense-Advanced Design Technology of Flight Vehicle, Nanjing University of Aeronautics and Astronautics, Nanjing 210016, P. R. China;
2. State Key Laboratory of Mechanics and Control of Mechanical Structures, Nanjing University of Aeronautics and Astronautics, Nanjing 210016, P. R. China

(Received 18 March 2015; revised 26 May 2015; accepted 23 June 2015)

Abstract: Optimization of the parameters of landing gear systems with double-stage air springs of catapult take-off carrier-based aircraft is here studied based on the mathematical equations of the classic dual mass spring-damper dynamic model. Certain standards for both take-off and landing performance are put forward. The contradictory factors between take-off and landing processes are analyzed. The optimization of oil in the pin area and the area near the rear oil hole is performed. Then these optimized parameters are used to assess the influence of the initial pressure of the low chamber, the ratio of the high chamber to the low chamber, and the tire inflation pressure on the performance of arresting landing and catapult take-off. The influences of these parameters on carrier-based aircraft and the aircraft-carrier on aircraft catapult take-off is also assessed. Based on the results of the simulation, respective take-off criteria must be drafted considering different types of aircraft and different take-off load cases, all of which must be matched to parameters relevant to catapult take-off.

Key words: carrier-based aircraft; buffer performance; fast-extension performance; aircraft design; optimization; sensitivity analysis

CLC number: V226 **Document code**: A **Article ID**: 1005-1120(2016)02-0187-12

0 Introduction

Carrier-based aircraft are different from ground-based aircraft. They must take off and land on an aircraft carrier, which is much smaller than conventional runways. Catapult take-off allows planes with heavier loads and longer ranges than ski-jump take-off does. Due to the limited length of the deck, carrier-based aircraft often use arrested landing (excepting vertical takeoff and landing aircraft). At the end of a catapult take-off process, the bumper of the nose landing gear extends quickly to pitch up the aircraft to the required angle of attack, therefore to generate the necessary lift[1,2]. Carrier-based aircraft also land much faster than normal aircraft. This arrested landing process calls for more energy absorption of landing gear than that of normal aircraft. Fast-extension performance and buffering performance are both crucial standards for the landing and the take-off of carrier-based aircraft.

(1) U. S. military standards and reports about the design of carrier-based aircraft landing gear are available for reference. U. S. military standard MIL-L-22589 provides details of the design, improvement, structure, analysis, experiment and relevant criteria and standards of the nose gear of carrier-based aircraft[3]. U. S. military standard MIL-A-8863 defines the strength

* Corresponding author, E-mail address: zhm6196@nuaa.edu.cn.

How to cite this article: Zhang Ming, Nie Hong, He Zhihang. Parameter optimization of nose landing gear considering both take-off and landing performance of catapult take-off carrier-based aircraft[J]. Trans. Nanjing Univ. Aero. Astro., 2016, 33(2):187-198.

http://dx.doi.org/10.16356/j.1005-1120.2016.02.187

and stiffness standards for carrier-based aircraft[4]. The Performance of five different models of carrier-based aircraft is discussed[5]. Other works expounded the principal theories and criteria for hold-down and release systems[6,7]. Researchers in China have thoroughly investigated multiple fast-extension modes, the effect of fast-extension on aircraft track, and the sensitivity parameters of the extension[8-14]. Concerning arresting landing, the arresting hook dynamics and load issue of landing gear have been studied[15,16]. However, contemporary studies have some limitations, for example, the research background has focused solely on fast-extension and bumping issues, and no thorough and systematic analysis on landing gear performance. Some research models used are not practical for engineering.

We, standing on the results of previous works, present a novel design for the nose landing gear of carrier-based aircraft and establish a dynamic model. The technology targets of nose landing gear performance are put forth with respect to both landing and catapult take-off. Optimization is conducted on the oil pin cross section and the size of back oil hole, which requires a trade-off between landing and catapult take-off performance. The sensitivity of the effect of nose landing gear filling parameters on landing and catapult take-off performance is analyzed based on optimization results.

1 Mathematic Model of Nose Landing Gear

1.1 Mechanics model of landing gear and relevant hypothesis

A structural figure of the landing gear buffering with double stage air chamber is shown in Fig. 1. A mechanical model of the landing gear based on the classic dual mass spring-damper model is shown in Fig. 2.

The air spring is used to absorb and reserve energy while the oil damper and friction damper are to dissipate energy. The mass of elastic supporting means the mass of the airframe along with the buffer's outer tub, while the mass of rigid supporting is comprised of the piston rod and wheel.

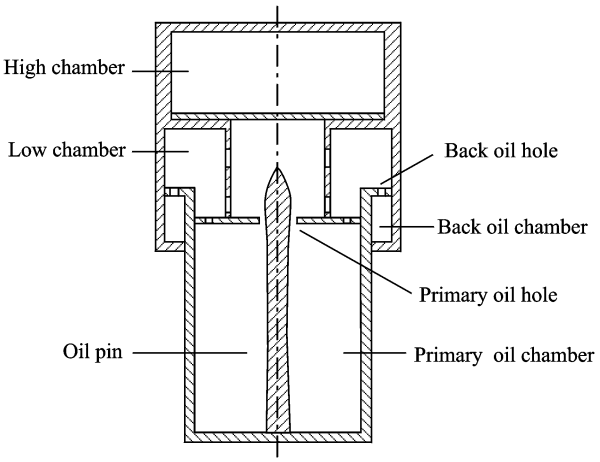

Fig. 1 Structure of damper with double-stage air spring

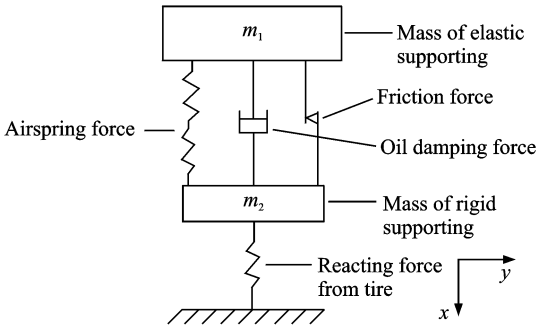

Fig. 2 Mechanical model of landing gear

In order to guarantee the precision of the calculations, we assume

(1) The effect of wheel spin-up is ignored.

(2) The axis of the buffer aligns with that of the landing gear.

1.2 Mathematical equations

The positive direction is along the axis of the damper downwards. Local coordinate system of elastic and rigid supporting is established, and the centers of mass of respective objects is set as the origins of coordinate. Then dynamic differential equations are constructed for the landing gear.

$$\begin{cases} m_1\ddot{x}_1 = m_1 g + T - F_a - F_{oil} - F_f - L \\ m_2\ddot{x}_2 = m_2 g - T + F_a + F_{oil} + F_f - F_v \end{cases} \tag{1}$$

The initial condition is as follows

$$\begin{cases} x_1 = x_2 = 0 \\ \dot{x}_1 = \dot{x}_2 = 0 \end{cases} \tag{2}$$

The boundary condition is as follows

$$x_1 - x_2 \leqslant s_{\max} \tag{3}$$

where m_1, m_2 are the mass of elastic supporting and rigid supporting mechanisms, respectively, and x_1, x_2 the displacements of elastic supporting mass and the rigid supporting mass, respectively. g is the gravitational acceleration, T the positive axial contact compression force between piston rod and outer tub (when damper is compressed, $T=0$), F_a the air spring force, F_{oil} the oil damping force, F_f the friction force between outer tub and piston rod, L the lift force, and F_v the supporting reaction force from deck to tire.

The equation for calculating air spring force is shown as follows

$$F_a = A_a\left[P_0\left(\frac{V_0}{V_0 - A_a \cdot S}\right)^{\gamma} - P_{atm}\right] \tag{4}$$

where A_a is the effective area of pressure in the air chamber, S the stroke of the damper, γ the gas polytropic index which varies between 1.1 and 1.4, and P_{atm} the air pressure. P_0, V_0 indicate the initial pressure and the volume of air in the chamber, respectively.

Calculation of oil damping force is given as follows

$$F_{oil} = \begin{cases} 0 & \dot{S} = 0 \\ \dfrac{|\dot{S}|\rho}{2\dot{S}}\left(\dfrac{A_h^3 \cdot \dot{S}^2}{C_d^2 \cdot A_d^2} + \dfrac{A_{hs}^3 \cdot \dot{S}^2}{C_{ds}^2 \cdot A_s^2}\right) & \dot{S} \neq 0 \end{cases} \tag{5}$$

where ρ is the density of the oil. C_d, C_{ds} are the coefficients of contraction of main oil chamber and back oil chamber, respectively, and A_h, A_{hs} the area of oil pressure of the main oil chamber and back oil chamber, respectively.

Equations for calculating friction force of leather cup is displayed as follows

$$F_f = \begin{cases} [K_m F_a + \mu_b(N_u + N_l)]\dot{S}/|\dot{S}| & \text{Damper bending} \\ K_m F_a \dot{S}/|\dot{S}| & \text{Damper not bending} \end{cases} \tag{6}$$

where K_m is the friction coefficient of leather cup and μ_b the bending friction coefficient of the damper. N_u, N_l are the normal forces of the upper and the lower supporting points when damper bends.

The processes of landing and catapult take-off are analyzed, and Eq. (1) is changed. During landing analysis, the time point when wheel just touches the deck with damper and the wheel is not compressed is set as initials. During catapult take-off analysis, the time point when the ejection force as just come into effect is set as initials.

1.3 Performance index for nose landing gear

Based on the working condition of the landing gear of carrier-based aircraft, two sets of performance index are put forward with respect to landing buffering and the fast extension of nose gear during take-off.

Landing buffering[17-19]:

(1) The landing gear damper ought to absorb work induced by the aircraft with a 7 m/s vertical landing speed in less than 0.8 s.

(2) The stroke of the damper should not exceed 90% of the max design stroke, and tire compression should not exceed 90% of the maximum, and tire force should remain in the linear phase. Only during rough landings should the damper or tire reach their respective limits.

(3) The damping system should be capable of absorbing the vibrations caused by repeated shock and prevent bouncing and wheel-deck separation.

Fast extension of nose gear during take-off[20, 21]:

(1) The extension should provide enough attack angle for a safe take-off within the length of deck before the nose wheel leaves the deck.

(2) After the ejection force disappears, nose landing gear must extend rapidly while the wheel is still in contact with the deck during the process.

(3) The extension time ought to be as short as possible, and it must end within the given length of deck.

Given the index above, several performance parameters are put forth as follows:

S is the stroke of the damper, l the load of the landing gear, and e the efficiency of the damper.

Parameters listed below are for analysis of

landing buffering.

t is the time of fast extension, d the displacement of fast extension, v the velocity of the mass of elastic supporting when extension ends, and α the attack angle when aircraft leaves deck.

2 Structural Parameter Contradictions and Relevant Optimization

2.1 Analysis on structural parameter contradictions

Structural parameters refer to the parameters of nose gear's main oil hole and rear oil hole. In order to control and configure the transient damping while working and to ensure the efficiency of the damper, the slope of the damper pillar force must remain to stroke figure positive. Therefore, the variable section main oil hole is used. A valve is installed to configure the positive and negative strokes of the damper.

The curves in Fig. 3 are the damping force of main oil hole and back oil hole during one stroke, respectively. During positive strokes, damping force generated by the main oil hole dominates, which indicates that main oil hole plays the main role in absorbing energy during landing. During negative strokes, the rear oil hole generates more damping force and prevents wheel from jumping and the damper from extending too fast.

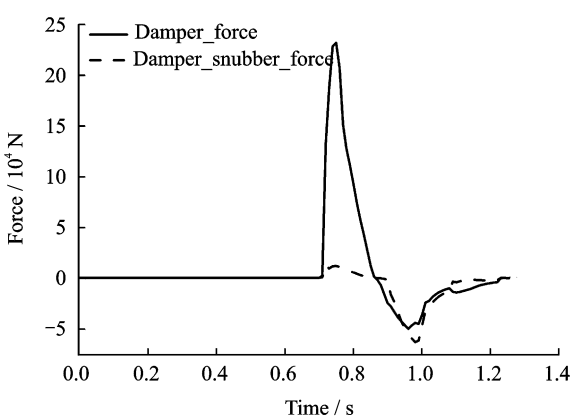

Fig. 3 Oil damping force

The damper absorbs at least 60% of the energy involved in the first compression while landing, which necessitates greater damping force from the main oil hole during the positive stroke and solid contact between the wheel and deck during the first negative stroke. This means a large oil damping joint force of negative stroke, which suggests a relatively small cross-section of the back oil hole during the negative stroke. For carrier-based aircraft, the fast extension period is during the negative stroke of damper, so fast extension requires a small damping for the negative stroke of damper, which necessitates a large cross-section of the negative stroke of rear oil hole.

2.2 Optimization on structural parameters

Based on the findings given in section 2.3, some key performance factors of landing buffering and the fast extension are here used as optimization objectives, as listed in Table 1, where F_d is the damping force of fast extension and n the maximum overload factor.

Table 1 Optimization objectives

Landing gear	Fast extension			Landing buffering	
	d	t	F_d	e	n
Nose	√	√	√	√	√
Main	×	×	×	√	√

The oil pin areas and oil hole areas in positive and negative strokes of the rear chamber here serve as design variables, as listed in Tables 2, 3.

The constraint functions of the optimization are as follows:

(1) The landing gear damper ought to absorb work induced by the aircraft at 7 m/s vertical landing speed in less than 0.8 s. The time required for one buffering stroke should be less than 0.3 s.

(2) The stroke of the damper must not exceed 90% of the max design stroke.

Table 2 Oil pin area of nose landing gear before optimization

Stroke variable	S_0	S_1	S_2	S_3	S_4	S_5	S_6	S_7	S_8	S_9	S_{10}	S_{11}	S_{12}
Stroke S/m	0	0.05	0.1	0.15	0.2	0.25	0.3	0.35	0.4	0.45	0.5	0.55	0.6
Oil pin area/cm^2	0	0.4	0.8	0.9	1.0	1.15	1.3	1.45	1.6	1.85	2.1	2.4	2.7

Table 3 Oil hole area of back chamber of nose landing gear before optimization

Oil hole area	Unoptimized
Positive stoke O_c/cm^2	4
Negative stoke O_c/cm^2	0.4

(3) The extension must provide a sufficient attack angle for a safe take-off within the length of deck before the nose wheel leaves the deck. The attack angle must be greater than 5°.

(4) The aircraft wheel should not rebound from the deck.

Integrate ADAMS/Aircraft software through simcode module of ISIGHT-fd system, the optimization procedure of nose gear damper structural parameters is given in Fig. 4.

We use non-linear quadratic programming method in ISIGHT-fd software to optimize the shape of oil pin and back oil. The most popular method of stroke-controlled cross-section of oil hole is faciliated by dividing the stroke into several phases. Then the shape of cross-section of the oil pin during the entire stroke can be put forward through quadratic curve fitting method. For rear oil hole parameters, the values of the range of areas for the stroke are given for the optimization process.

Optimization is conducted in two ways, one for landing alone, and another is for landing and fast extension. The optimized oil pin area and the oil hole area of the rear chamber of the nose landing gear are shown in Tables 4, 5.

The optimized figure of the buffer is shown in Fig. 5.

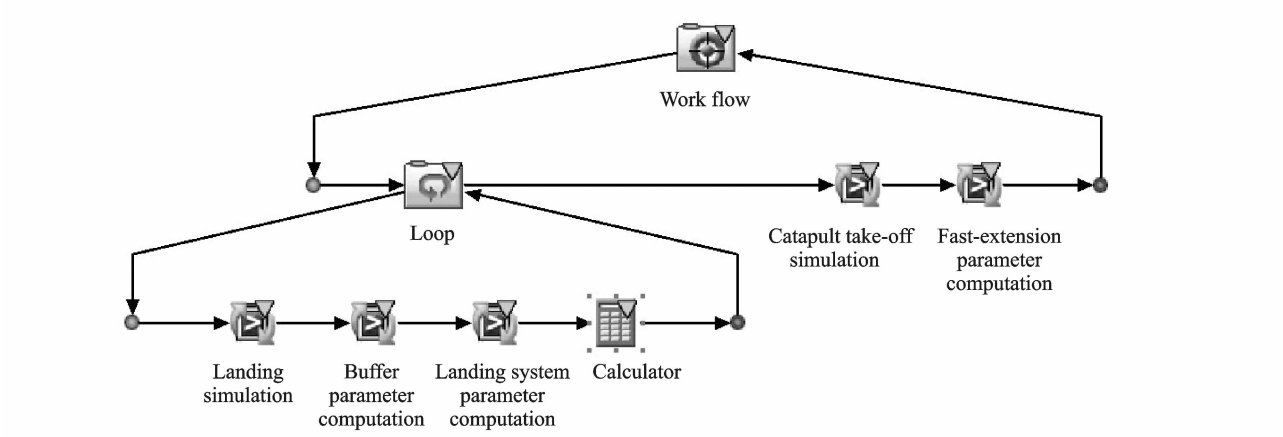

Fig. 4 Optimization procedure of nose gear damper structural parameters

Table 4 Oil pin area of nose landing gear after optimization

Stroke variable	S_0	S_1	S_2	S_3	S_4	S_5	S_6	S_7	S_8	S_9	S_{10}	S_{11}	S_{12}
Stroke S/m	0	0.05	0.1	0.15	0.2	0.25	0.3	0.35	0.4	0.45	0.5	0.55	0.6
Optimized for landing	0	0.4	1.37	1.29	1.27	1.32	1.29	1.33	1.51	1.67	1.83	2.23	2.57
Optimized for landing and fast extension	0	0.5	1.35	1.22	1.22	1.22	1.22	1.12	1.38	1.48	1.87	2.34	2.68

Table 5 Oil hole area of the rear chamber of nose landing gear after optimization

Oil hole area	Optimized for landing	Optimized for landing and fast extension
Positive stoke O_c/cm^2	4	4
Negative stoke O_c/cm^2	0.8	2

Fig. 5 shows that landing performance after optimization is better than the unoptimized; And the one only optizmized for landing is better than that optimized both for landing and fast extension. The axial force of the damper during the negative stroke on the condition of landing is smaller than that for both landing and take-off. This shows that a rapid rise in the nose while taking off could be easier to effect.

Fig. 6 depicts the curve of attack angle while

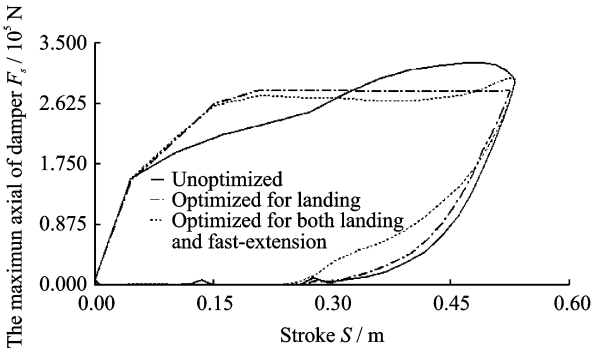

Fig. 5 Working of the damper

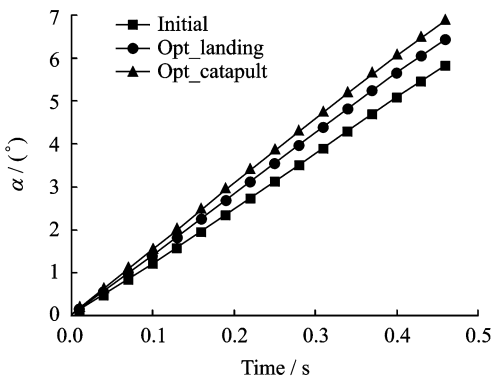

Fig. 6 Attack angle over time while leaving deck

the plane is leaving the deck. After optimization, the attack angle increases, which means the aircraft can generate more lift force while leaving the deck.

The objectives for landing gear are optimized in two ways, based on initial structural parameters and on two groups of optimized parameters. Results are shown in Table 6.

Table 6 Optimization objectives of nose landing gear

Case performance		Initial	Opt_landing	Opt_catapult
Landing	s/mm	544	532	532.1
	l/kN	326.3	295.5	298.5
	e	0.721	0.827	0.812
Catapult	t/s	0.18	0.17	0.18
	d/mm	252.1	307.7	346.6
	v/(m·s^{-1})	2.31	2.62	2.82
	α/(°)	4.21	5.08	5.51

Several conclusions can be drawn from the data in Table 6. For landing, the optimized structure can decrease the landing gear overload and increase the efficiency of damper by 10%. For take-off and fast-extension, length is increased by 90 mm within the length of deck.

3 Sensitivity of Filling Parameters

While designing the landing gear, filling parameters should include initial inflation pressure of low chamber P_{L0} and that of high chamber P_{H0}; Initial volume of low chamber V_{L0} and that of high chamber V_{H0}, and tire inflation pressure V_t. Nevertheless, these parameters are not all independent of each other. It is here suggested that the stroke of the damper is a constant value. Then the pressure of chambers and inflation volume of chambers are connected to each other through gas state equations. Moreover, inflation pressure in the high and low chambers is related to the transition stroke. For this reason, the sensitivity of relevant parameters is analyzed in this paper.

3.1 Initial pressure of the low chamber

As shown in Table 7, when initial inflation pressure increases from 1.13 MPa to 2 MPa, maximum axial force of damper during landing drops by 10 kN, damper efficiency increases by 5%, and the stroke of the damper decreases by around 17 mm, which indicates that increasing the initial pressure of low chamber boosts the performance of the damper. In terms of fast extension performance, as initial pressure of the low chamber increases, the time of extension increases by 0.3 s. The axial velocity of upper supporting mass increases somewhat, with a 70 mm increase of the extension length. Nevertheless, velocity of aircraft while leaving deck does not increase with the increase of inflation pressure. With the limited length of the deck, the off-ship attack angle become the key parameter for take-

Table 7 Effect of initial pressure of the low chamber

P_{L0}		1.13	1.3	1.5	1.73	2
Landing	s/mm	539.6	536.3	532.1	527.8	522.9
	l/kN	303.9	301.3	298.5	296.0	293.1
	e	0.787	0.80	0.812	0.827	0.84
Catapult	t/s	0.17	0.18	0.18	0.19	0.2
	d/mm	325.8	351.4	346.6	371.1	396.5
	v/(m·s^{-1})	2.81	2.81	2.82	2.82	2.83
	α/(°)	5.37	5.38	5.51	5.35	5.37

off analysis. As a result, both increases and decreases in initial pressure of the low chamber leads only to disadvantages.

3.2 Initial pressure of the high chamber

As shown in Table 8, as the ratio increases from 3.5 to 7.2, the maximum axial force of the damper during landing increases by 46 kN, the efficiency of the damper drops by 7%, with a decrease in damper stroke of 54 mm. This indicates that a greater ratio brings a weaker performance for buffering. In terms of fast extension performance, as the ratio increases, time of extension occurres 0.5 s earlier. Although extension length shrink by 95 mm, the axial velocity of upper supporting mass at the end of extension increases by 0.23 m/s, and the off-ship attack angle increases by 1.2°. This suggests that a high ratio between pressure of high chamber and low chamber may improve the performance of fast extension.

Table 8 Initial pressure of the high chamber

Initial pressure		3.5	4.2	5	6	7.2
Landing	s/mm	558.1	546.2	532.1	518.7	504.6
	l/kN	281.5	288.5	298.5	310.8	327.1
	e	0.836	0.827	0.812	0.794	0.766
Catapult	t/s	0.21	0.2	0.18	0.17	0.16
	d/mm	418.8	394.7	346.6	332.6	323.2
	v/(m·s^{-1})	2.69	2.76	2.82	2.87	2.92
	α/(°)	4.79	5.05	5.51	5.71	6.08

3.3 Tire pressure

As shown in Table 9, as the tire pressure increases from 1.5 to 2.2, the maximum axial force of the damper during landing decreases by 7.6 kN, the efficiency of the damper increases by 2%, with a decrease in damper stroke of 2.4 mm. The efficiency of the entire damping system increases by about 3%, so increases of the initial pressure of the lower chamber has good effects on damping performance. However, when tire pressure is below 1.65 MPa, tire compression does not remain linear stage. With respect to fast extension performance, extension takes place 0.1 s earlier as pressure increases. The axial velocity of the upper supporting mass at the end of extension drops slightly, and the off-ship attack angle decreases by 0.05° with a 34 mm increase in the length of extension. It can be concluded that low tire pressure leads to better performance of fast extension, but the effect is limited. Tire force may exceed its linear stage due to insufficient tire pressure, so it must maintain a suitable value and damping performance must be taken into serious consideration.

Table 9 Tire pressure

Tire pressure		1.5	1.65	1.81	2.0	2.2
Landing	s/mm	534.5	533.9	533.4	532.8	532.1
	l/kN	306.1	304.1	302.3	300.4	298.5
	e	0.789	0.794	0.799	0.806	0.812
Catapult	t/s	0.19	0.19	0.19	0.18	0.18
	d/mm	381.1	379.8	376.6	347.3	346.6
	v/(m·s^{-1})	2.87	2.85	2.84	2.83	2.82
	α/(°)	5.56	5.55	5.53	5.52	5.51

4 Parameter Match Between Carrier-Based Aircraft and Aircraft-Carrier

Parameter matches between carrier-based aircraft and the aircraft carriers refers to parameters concerning ejection force provided by aircraft catapult, the length of take-off runway, wind over the deck when carrier cruises windward, initial load of the aircraft, and the trust force of engine. Initial parameters shared between carrier-based aircraft and the aircraft-carrier are used for analysis as listed in Table 10.

Table 10 Initial parameters for simulations

Parameter	Value
Ejection force of catapult/PSI	600
Length of carrier runway/m	103
Aircraft mass/kg	33 000
Aircraft thruster force/kN	252.16

4.1 Ejection force

The American C13-1 catapult is used for the analysis for the simulation, as there are neither relevant standards nor steam catapult in this country. In the simulations, initial parameters of deck length, aircraft mass, and engine thrust force are applied. Wind over the deck is disregarded, and the ejection force of catapult is changed by 10% each time, and three different curves of force-stroke are given, as shown in Fig. 7. The

effect of thrust force on take-off performance is here analyzed by harnessing these data. Results are listed below.

Based on Table 11 and Figs. 7—11, it is evident that as ejection force increases from 545 PSI to 660 PSI, off-deck time of nose wheel starts 0.2 s earlier, off-deck velocity increases by 5.4 m/s, and the off-deck attack angle drops by 0.4°. This explains that large ejection force grants a higher acceleration during the take-off run, and the aircraft leaves the deck so quickly that nose gear can not make full contact with the deck, which leads to an insufficient fast-extension. As ejection force increases, the maximum axial force of the nose damper increases by 67 kN and maximum axial force of main damper increases by 47 kN, due to an increasing component of force along axial direction. When ejection force reaches 545 PSI, the deflection quantity reaches 0.91 m and does not exceed 3 m. After leaving the deck, the vertical velocity of the aircraft is lower than 3 m/s, so the take-off process still results in failure in this case.

Note that the aircraft fails to take off when ejection force reaches the maximum value, a large off-deck attack angle still benefits the take-off process. This is because the taxi run velocity is so short that the aircraft stays on the deck too long, which guarantees a large off-deck attack angle. However, after leaving the deck, the attack angle fails to compensate for the negative effects of the low off-deck velocity and the loss of the ground effect.

Table 11 Simulation results under different ejection forces

Ejection force of catapult	Off-deck time of nose wheel/s	Off-deck velocity/(m·s^{-1})	Off-deck attack angle/(°)	Maximum axial force of nose damper/N	Maximum axial force of main damper/N	Deflection quantity/m
545PSI	2.81	72.2	2.18	3.32×10^5	3.42×10^5	0.91
600PSI	2.71	74.7	2.02	3.66×10^5	3.63×10^5	0.26
660PSI	2.61	77.6	1.79	3.99×10^5	3.89×10^5	—

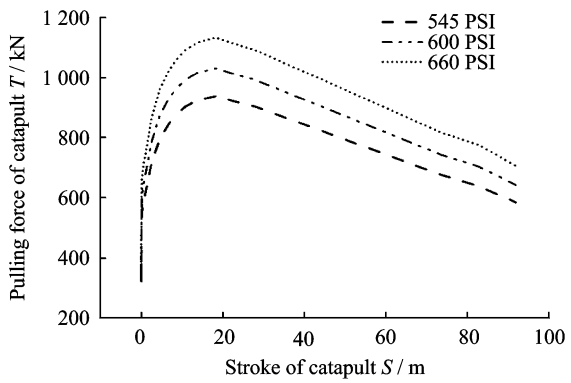

Fig. 7 Pulling forces over stroke under different ejection forces

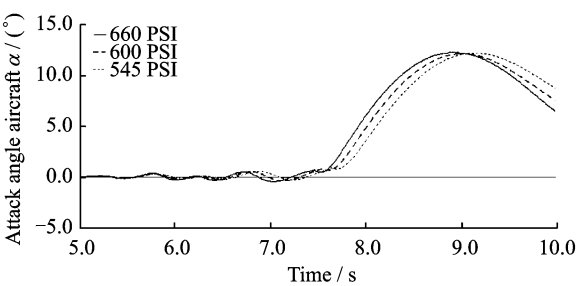

Fig. 8 Attack angles under different ejection forces

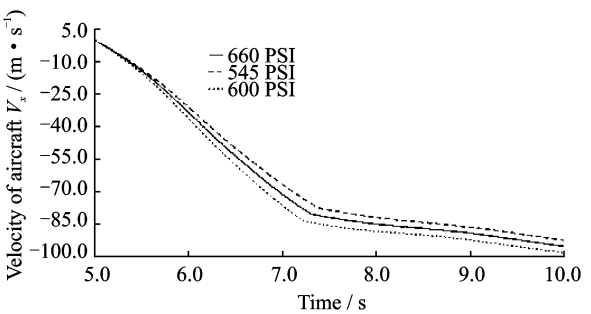

Fig. 9 Velocities under different ejection forces

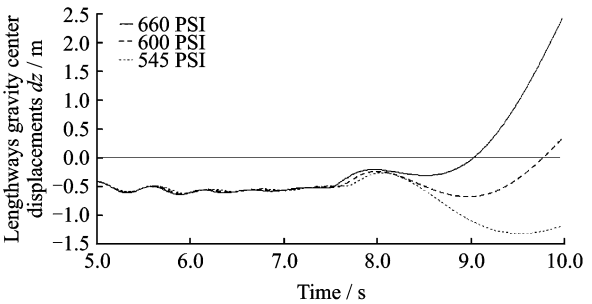

Fig. 10 Lengthways gravity center displacements under different ejection forces

4.2 Deck length

During catapult take-off, the end of the

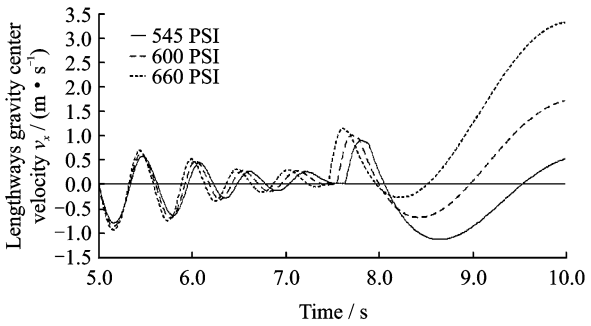

Fig. 11 Lengthways gravity center velocities under different ejection forces

stroke of the catapult does not reach the end of the deck. The distance between them ranges from 5.8 m to 44.2 m. This interval profoundly affects how long the ground effect lasts after ejection force disappears, as well as the time of contact between the wheel and the deck. Therefore, this interval is important for the analysis of off-deck attack angle and deflection quantity of flight path.

Initial parameters of aircraft mass, engine thrust force, ejection force of the catapult are applied, the wind over the deck is ignored, and three sets of deck length are put forth: d_1 = 103 m, d_2 = 115 m, d_3 = 127 m. The effect of deck length on performance of take-off is analyzed based on these sets of data.

Conclusions can be drawn (See Table 12). With the increase in deck length, the nose wheel can leave deck safely, the off-deck velocity increases by 1.7 m/s, the off-deck attack angle increases by 3°, and the maximum axial force of both nose and main landing gear remains unchanged. The deflection of flight path gradually decreases to zero. In conclusion, extending deck length is a fine option for increasing off-deck speed and off-deck attack angle and providing sufficient ground effect. A long deck is also good for the flight path and boosts take-off performance.

4.3 Mass at take-off

Initial parameters of length of deck, engine thrust force, ejection force of catapult are used, and wind the over deck is ignored. Three sets of take-off loads are here put forth: m_1 = 25 000 kg, m_2 = 29 000 kg, m_3 = 33 000 kg. Analysis of the effect of take-off mass on take-off performance is conducted based on the previous sets of data.

It is deduced from Table 13 that off-deck time of nose wheel is put off by 0.5 s and the off-deck velocity decreases by 14.6 m/s as take-off load increases from 25 000 kg to 37 000 kg, because the acceleration of the aircraft drops due to the increasing load and invariant ejection force and deck length. Therefore, the velocity ejector delivered to the aircraft is greatly limited, and aircraft lingers longer on the deck. The smallest off-deck attack angle is observed when take-off load is 25 000 kg, because the aircraft does not stay on the deck long enough, leading to an insufficient fast-extension. As the take-off load reaches 37 000 kg, its off-deck attack angle decreases instead of increasing because of the relatively low off-deck velocity. As the take-off load increases, so does the maximum axial force of both nose and main dampers. When take-off load reaches 37 000 kg, the deflection of off-deck flight path exceeds 3 m, and the vertical upward velocity of aircraft fails to increase, which causes it to fail.

Among the sets of data applied in the simulations, the minimum off-deck attack is observed when aircraft mass does not exceed 25 000 kg, but there is no deflection of flight path. This can be attributed to the fast off-deck velocity and the upward vertical velocity continuing to increase after leaving the deck, as does the attack angle, which facilitates safe take-off by offering sufficient lift force against gravity.

4.4 Engine thrust force

If the length of deck is inadequate, the flight path is deflected. To ensure safe take-off, engine thrust force must be able to maintain enough thrust force to enable the aircraft to climb after a period of descent 3 s after reaching maximum deflection. Engine thrust force depends only on engine attributes.

Initial parameters of aircraft mass, deck length, and ejection force of catapult, are used. the wind over the deck is disregarded, and four

sets of deck length are applied by configuring thrust 20% at a time: $T_1 = 174.2$ kN, $T_2 = 209.7$ kN, $T_3 = 250.88$ kN, $T_4 = 301.06$ kN. The effect of engine thrust force on take-off performance is analyzed using such sets of data.

It is concluded from Table 14 that, as the engine thrust force increases from 174.2 kN to 301.06 kN, off-deck time of nose wheel takes place 0.2 s earlier, and off-deck velocity drops by 5.47 m/s. This is primarily because the increment of thrust force significantly increases the acceleration under the invariant ejection force and take-off mass. As a result, the velocity of aircraft at the end of deck and the off-deck attack angle both increase, and the time range during which the aircraft remains on the deck decreases. The maximum axial force of the nose gear increases, and that of main landing gear decreases, but the variations are limited. If thrust force is under 250.88 kN, flight path is deflected after the aircraft leaves the deck. When the force is equal to 174.2 kN, aircraft drops profoundly after the aircraft left the deck and fails to climb up. When thrust force is 209.7 kN, the deflection of flight path is 1.13 m, which does not exceed 3 m. However the rate of climbing does not reach 3 m/s within 3 s of leaving the deck. This is an unsuccessful take off.

Table 12 Simulation results at different deck lengths

Deck length/m	Off-deck time of nose wheel/s	Off-deck velocity/(m·s^{-1})	Off-deck attack angle/(°)	Maximum axial force of nose damper/N	Maximum axial force of main damper /N	Deflection quantity/m
103	2.71	74.7	2.02	3.66×10^5	3.63×10^5	0.26
115	2.75	75.6	3.59	3.66×10^5	3.63×10^5	—
127	2.75	76.4	5.01	3.66×10^5	3.63×10^5	—

Table 13 Simulation results with different take-off loads

Take-off load/10^3 kg	Off-deck time of nose wheel/s	Off-deck velocity/(m·s^{-1})	Off-deck attack angle/(°)	Maximum axial force of nose damper/N	Maximum axial force of main damper /N	Deflection quantity/m
25	2.37	85.3	1.02	3.17×10^5	3.11×10^5	—
29	2.55	79.5	1.62	3.45×10^5	3.37×10^5	—
33	2.71	74.7	2.02	3.66×10^5	3.63×10^5	0.26
37	2.87	70.7	1.82	3.82×10^5	3.93×10^5	Failure

Table 14 Simulation results under different thruster forces

Thruster force of engine/kN	Off-deck time of nose wheel/s	Off-deck velocity/(m·s^{-1})	Off-deck attack angle/(°)	Maximum axial force of nose damper/N	Maximum axial force of main damper /N	Deflection quantity/m
174.2	2.83	71.36	1.86	3.74×10^5	3.57×10^5	Failure
209.7	2.77	72.92	1.91	3.71×10^5	3.60×10^5	1.13
250.88	2.71	74.7	2.02	3.66×10^5	3.63×10^5	0.26
301.06	2.64	76.83	2.09	3.60×10^5	3.67×10^5	—

5 Conclusions

(1) Nose landing gear performance is explored with respect to both landing and catapult take-off. Optimization of the oil pin cross-section and the size of back oil hole can necessitate a tradeoff between landing and catapult take-off performance. Optimized structure can decrease the landing gear overload and increase the efficiency of buffer by 10%. For take-off, fast-extension length is increased by 90 mm within the length of the deck.

(2) Inflation pressure in the low air chamber has little effect on buffering or fast-extension performance. It is unwise to modify its parameters in practical situations. Inflation pressure in the high air chamber has profound effects on fast-extension performance, the higher the pressure, the

better the fast-extension performance. Nevertheless, if pressure grow too high, the buffering effect is weakened. Lower tire pressure will be good for fast-extension performance to an extent. Considering that a high tire pressure prevents the tire from entering a nonlinear stage, the value of inflation pressure tends not to be too low, and buffering performance should be taken into consideration.

(3) Match parameters between carrier-based aircraft and aircraft-carriers affect each other. Larger ejection forces and thrust force benefit off-deck velocity. However, if the deck is too short, this ejection force and thrust force can cause only a small off-deck attack angle. Extended deck length can compensate for the inadequate thrust force and ejection force. Safety criteria specific to different types of aircraft and types of take-off loads must be established with several ejection parameters modified for their specific cases.

Acknowledgements

This work was supported by the National Natural Science Foundation of China (Nos. 51305198, 11372129).

References:

[1] PATTERSON D, MONTI A, BRICE C, et al. Design and simulation of an electromagnetic aircraft launch system[C]// Industry Applications Conference. Pittsburgh, PA, USA: [s. n.], 2002: 1950-1957.

[2] BUSHWAY R. Electromagnetic aircraft launch system development considerations[J]. Magnetics, IEEE Transactions on, 2001, 37(1): 52-54.

[3] Naval Air Engineering Center. Launching system, nose gear type, aircraft, Specification M: MIL-L-22589D(AS)[S]. Lakehurst NJ: [s. n.], 1979.

[4] Naval Air Engineering Center. Military specification: Airplane strength and rigidity ground loads for navy acquired airplanes: MIL-A-8863C(AS)[S]. Lakehurst NJ: [s. n.], 1993.

[5] LUCAS C B. Catapult criteria for a carrier-based aircraft: AD702814[R]. USA: [s. n.], 1968.

[6] Naval Air Engineering Center. Tension bar/release element, aircraft launching: MIL-T-23426D(AS)[S]. Lakehurst NJ: [s. n.], 1986.

[7] Naval Air Engineering Center. Bar, repeatable release holdback (RRHB), aircraft launching, general requirement for use on carrior-type aircraft: MIL-DTL-85110B(AS)[S]. Lakehurst NJ: [s. n.], 1997.

[8] SHEN Qiang, HUANG Zaixin. Sensitivity analysis of fast-extension performance of carrier based aircraft landing gear to varying parameters[J]. Acta Aeronautica et Astronautica Sinica, 2010, 31(3): 532-537. (in Chinese)

[9] HUANG Zaixin, FAN Weixun, GAO Zejiong. Dynamic analysis of nose gear fast-extension of carrier based aircraft[J]. Journal of Nanjing University of Aeronautics and Astronautics, 1995, 27(4): 466-473. (in Chinese)

[10] HU Shuling, LIN Guofeng. The effects of nose landing gear jump on the carrier aircraft catapult take-off flight path[J]. Flight Dynamics, 1993, 12(1): 28-34. (in Chinese)

[11] LIU Xingyu, XU Dongsong, WANG Lixin. Match characteristics of aircraft-carrier parameters during catapult take off of carrier-based aircraft[J]. Acta Aeronautica et Astronautica Sinica, 2010, 31(1): 102-108. (in Chinese)

[12] JIN Changjiang, HONG Guanxin. Dynamic problems of carrier aircraft catapult launching and arrest landing[J]. Acta Aeronautica et Astronautica Sinica, 1990, 11(12):534-542. (in Chinese)

[13] YU Hao, NIE Hong. Launch bar load analysis of carrier-based aircraft during off-center catapult launch [J]. Acta Aeronautica et Astronautica Sinica, 2010, 31(10):1953-1959. (in Chinese)

[14] YU Hao, NIE Hong, WEI Xiaohui. Analysis on the dynamic characteristics of carrier-based aircraft nose landing gear with sudden holdback load discharge[J]. Acta Aeronautica et Astronautica Sinica, 2011, 32(8):1435-1444. (in Chinese)

[15] LIU Gang, NIE Hong. Dynamics of arresting hook bounce after initial touchdown and impacting with deck[J]. Acta Aeronautica et Astronautica Sinica, 2009, 30(9):1672-1676. (in Chinese)

[16] LIU Gang, NIE Hong. Dynamics of bounce of aircraft arresting hook impacting with deck and performance of arresting hook longitudinal damper[J]. Acta Aeronautica et Astronautica Sinica, 2009, 30(11):2093-2098. (in Chinese)

[17] WEI Xiaohui, NIE Hong. Study on landing impact force of carrier based aircraft landing gears[J]. China Mechanical Engineering, 2007, 18(5):520-523. (in Chinese)

[18] WANG Qiansheng. A preliminary research of sinking velocity for carrier-based aircraft[J]. Aircraft Design, 2007, 27(3): 1-6. (in Chinese)

[19] LI Bo, SHEN Hang. Determination to maximum aircraft sinking speed[J]. Chinese Journal of Applied Mechanics, 2008, 25(1): 169-171. (in Chinese)

[20] ZHAO Bo. Flight dynamic problems of carrier aircraft during takeoff and landing[J]. Flight Dynamics, 1991(4):83-89. (in Chinese)

[21] XU Yan. Dynamic study of ski-jump takeoff of carrier-based aircraft[D]. Nanjing, China: Nanjing University of Aeronautics and Astronautics, 2008. (in Chinese)

Dr. **Zhang Ming** is currently an associate professor in College of Aerospace Engineering, Nanjing University of Aeronautics and Astronautics. He received his Ph. D. degree in Aircraft Design from Nanjing University of Aeronautics and Astronautics in 2009. His research interests include aircraft design, dynamics and landing gear system.

Dr. **Nie Hong** is currently a professor and doctoral supervisor in Nanjing University of Aeronautics and Astronautics. He received his Ph. D. degree in Aircraft Design from Nanjing University of Aeronautics and Astronautics in 1992. His current research interests include aircraft design, dynamics and landing gear system.

Mr. **He Zhihang** is currently a M. S. candidate in Nanjing University of Aeronautics and Astronautics. His current research interests include aircraft design, dynamics and landing gear system.

(Executive Editor: Xu Chengting)